SPECTRAL MULTIPLEXING USING QUANTUM DOT TAGGED MICROSPHERES WITH DIFFUSING COLLOIDAL PROBE MICROSCOPY

A Thesis

by

SHANKARAPANDIAN MUTHUKUMAR

Submitted to the Office of Graduate Studies of
Texas A&M University
in partial fulfillment of the requirements for the degree of

MASTER OF SCIENCE

May 2007

Major Subject: Biomedical Engineering

SPECTRAL MULTIPLEXING USING QUANTUM DOT TAGGED MICROSPHERES WITH DIFFUSING COLLOIDAL PROBE MICROSCOPY

A Thesis

by

SHANKARAPANDIAN MUTHUKUMAR

Submitted to the Office of Graduate Studies of
Texas A&M University
in partial fulfillment of the requirements for the degree of

MASTER OF SCIENCE

Approved by:

Chair of Committee,	Kenith E.Meissner
Committee Members,	Michael A.Bevan
	Gerard L.Coté
Head of Department,	Gerard L.Coté

May 2007

Major Subject: Biomedical Engineering

ABSTRACT

Spectral Multiplexing Using Quantum Dot Tagged Microspheres with Diffusing Colloidal Probe Microscopy. (May 2007)

Shankarapandian Muthukumar, B.E, University of Madras

Chair of Advisory Committee: Dr. Kenith E.Meissner

This work involves the development of a new technique that integrates Diffusing Colloidal Probe Microscopy (DCPM) and luminescence to simultaneously measure multiple particle-wall interactions. DCPM can be used to map potential energy profiles of multiple particle-surface interactions simultaneously and accurately. Colloidal semiconductor quantum dots were used for spectral multiplexing to enable monitoring of multiple analytes at the same time.

DCPM combines Total Internal Reflection Microscopy (TIRM) and Video Microscopy to simultaneously measure multiple particle-surface interactions with nanometer resolution in particle-surface separation. By acquiring the scattered intensity emitted by the particles, the separation distance can be calculated and subsequently the forces of interactions between the particle and the surface.

This work demonstrates the use of luminescence instead of scattering as the mode of detection in DCPM. The luminescence is provided by quantum dots which are incorporated into polystyrene microspheres. The unique optical properties of quantum dots enable the creation of an optically multiplexed system where microspheres are tagged by quantum dots of different emission wavelengths.

Scattering in DCPM may result in erroneous calculation of the potential energy profiles because of particle polydispersity. Since scattering is dependent on particle size, luminescence is introduced into the system and some interesting results are obtained. These results illustrate that the effect of particle polydispersity is significantly reduced when luminescence is used as the mode of detection. This combined with the DCPM system's sensitivity would enable the monitoring of multiple functionalized particle-surface interactions simultaneously and accurately.

To my caring mother, inspirational father, influential sister and loving grandparents

ACKNOWLEDGMENTS

I would like to thank my advisor Dr.Kenith Meissner who has been patient with me while guiding me through my Master's program. I would also like to thank Dr.Michael Bevan and his research group, especially Neil Everett and Richard Beckham who helped me all the way in getting this work done successfully despite their busy schedules. I am also grateful to Bhavik Nathwani and Haribhaskar Balasubramanian, who took time off from their schedule to help me synthesize quantum dots used in this work.

TABLE OF CONTENTS

Page

Page

LIST OF FIGURES

FIGURE Page

NOMENCLATURE

QD	Quantum Dot
CdSe	Cadmium Selenide
ZnS	Zinc Sulfide
TOPO	Trioctylphosphine oxide
TIRM	Total Internal Reflection Microscopy
DCPM	Diffusion Colloidal Probe Microscopy
EW	Evanescent Waves

INTRODUCTION

This work involves the development of a new technique that integrates Diffusing Colloidal Probe Microscopy (DCPM) and luminescence to simultaneously measure multiple particle-wall interactions. DCPM can be used to map potential energy (PE) profiles of the particle-surface interactions and hence, deduce the forces of interactions between the particles and the surface. The optical properties of quantum dots make spectral multiplexing possible where polystyrene microspheres tagged by different-sized quantum dots are spectrally distinct and simultaneously monitored.

Colloidal particles undergo Brownian motion and their distance from the wall fluctuates continuously.[1] Consequently, there is a need for a method to observe the particle-wall interactions during Brownian motion, and this is accomplished by our DCPM system. DCPM combines Total Internal Reflection Microscopy (TIRM) and Video Microscopy to simultaneously measure multiple particle-surface interactions with nanometer resolution in particle-surface separation.[2] By acquiring the scattered intensity from the particles, the separation distance can be calculated using methods explained in subsequent sections.

The efficiency of the DCPM system can be improved using luminescence from quantum dots embedded in microspheres instead of scattering from the particles. The

---

This thesis follows the style of *Langmuir*.

narrow emission and broad absorption spectra of quantum dots (QD's) make spectral multiplexing a viable technique to be integrated with DCPM. This combined with the DCPM system's sensitivity would enable the monitoring of multiple functionalized particle-surface interactions simultaneously.

A major concern in the DCPM system is particle polydispersity. This may result in erroneous calculation of the PE profile as scattering is dependent on particle size.[3] Using quantum dot luminescence as mode of detection in the DCPM could result in particle polydispersity playing less of a role in potential energy and force calculations.

So, we synthesize quantum dots with different luminescent wavelengths and embed them in polystyrene microspheres. This enables a parallel, high-throughput analysis of multiple particle-surface interactions using the DCPM system and at the same time, might reduce the effects created by particle polydispersity.

BACKGROUND

QUANTUM DOTS

Quantum Properties

In order to understand the physics of quantum dots, one must understand the band theory of solids. In atoms, the energy levels of electrons are quantized. When two or more atoms are brought together to form a molecule, the energy levels of electrons from individual atoms are very close to each other and hence experience a higher inter-atomic interaction potential. When the number of atoms in a molecule is very large, energy bands are formed with very small spacing between these energy levels. These bands may be empty or partially filled or completely filled with electrons, governed by Pauli's exclusion principle.[4]

Empty bands do not contain electrons and therefore do not contribute to the electrical conductivity of the material. Partially filled bands contain electrons as well as unoccupied energy levels of slightly higher energy, which enable carriers to gain energy when moving in an applied electric field. Electrons in a partially filled band therefore contribute to the electrical conductivity of the material. Completely filled bands contain plenty of electrons but do not contribute to the conductivity of the material as the electrons cannot gain energy since all energy levels are already filled.

The distinct energy bands in a material are called the valence band and conduction band.

Valence Band

The valence band is the highest filled band of allowed energy states. Since electrons have a tendency to fill the lowest available energy states, the valence band is always nearly completely filled with electrons, especially as the temperature falls towards 0 K. As the temperature rises or when excited with light, electrons can absorb the energy and leave the valence band and be promoted to the conduction band, which is the upper band of allowed states, provided this energy is greater than the energy gap between the valence and conduction bands of the material.

Conduction Band

The conduction band is usually empty and contains few or no electrons since energy is required for them to get there from the valence band. When an electron gains sufficient energy, greater than the band gap energy of the crystal, and gets to the conduction band, it is free to move becoming a carrier and therefore, increases the conductivity of the material. The average lifetime of electrons in a conduction band is a small fraction of a second. Since this is the band where the electrons contribute towards the conduction of the material, it is called the conduction band. When the electron loses its energy, it drops back down to the valence band emitting its energy as heat, light or by transferring it to another electron.

The energy bands in different types of materials are shown in Figure 1.[5] In insulators, the valence band is full and is separated by a large energy gap from the conduction band. So, the electrons must possess enough energy to bridge this gap in order to conduct electricity. In conductors like metals, the valence band overlaps the

conduction band and hence, the electrons are free to move between the two bands conducting electricity. In semiconductors, the energy gap between the valence and conduction bands is small enough that thermal or other excitations can bridge the gap making it possible for electrons to move freely.

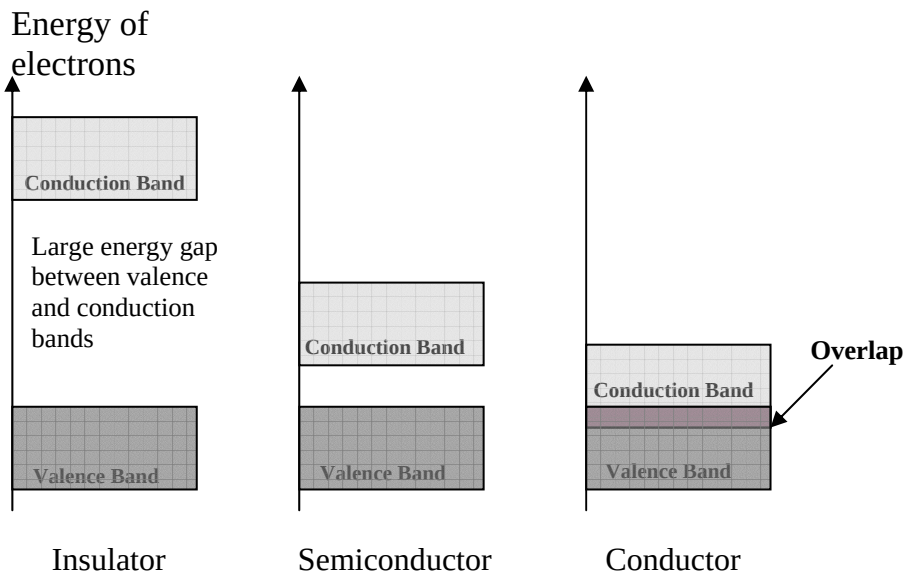

Figure 1. Energy Bands in Solids.[5]

The energy gap determines the wavelength of light required to facilitate the excitation of electrons to the conduction band and also, determines the wavelength that is emitted by the material when the electrons fall back to the valence band. This gap is fixed for a particular material, and hence the absorption and emission spectra are also constant.[6]

When an electron leaves the valence band, it leaves behind a vacant position in the crystal called hole, which can move about the crystal, adding to the conductivity of the material. The excited electron and its corresponding hole are bound to each other by

an electrostatic attraction to form an exciton. Excitons have an average physical separation between the electron and hole, referred to as the Exciton Bohr Radius which is different for each material. In bulk, the dimensions of the semiconductor crystal are much larger than the Exciton Bohr Radius, allowing the exciton to extend to its natural limit. However, if the size of a semiconductor crystal becomes smaller than the material's Exciton-Bohr Radius, then the electron/hole pairs are said to be confined in that dimension and the phenomenon is called quantum confinement.[7] The quantum confinement effect results in altered optical properties of quantum dots and allows tuning of their absorption and emission spectra as a function of size.

The quantum confinement principle along with the corresponding density of states is shown in Figure 2 where E represents the energy of the material with g(E) corresponding to density of states of that material.[8]

Confinement in 1-dimension

Sandwiching a narrow-bandgap material between two large-bandgap materials creates quantum wells.[9] Such a system confines the electrons to move between the two materials making the energy levels quantized in accordance with the thickness of the material. Figure 2 shows confinement of a material and its corresponding density of states. Also, there is a shift in the absorption and emission spectra of the sandwiched material toward the blue due to increased self-energy. [10]

Confinement in 2-dimensions

Confining the electrons in 2-dimensions results in quantum wires where the energy levels are confined in a second dimension, causing the excited electrons and their

corresponding holes to be spatially confined and making the energy states within the bands compressed. Figure 2 shows this confinement.

Confinement in 3-dimensions

In the case of a quantum dot, the motion of electrons is restricted in all three dimensions[11] resulting in discrete energy states, thereby increasing the density of states as shown in Figure 2 and causing another shift in the emission wavelength. It is because of this the QD's are also known as 0-D structures or artificial atoms.

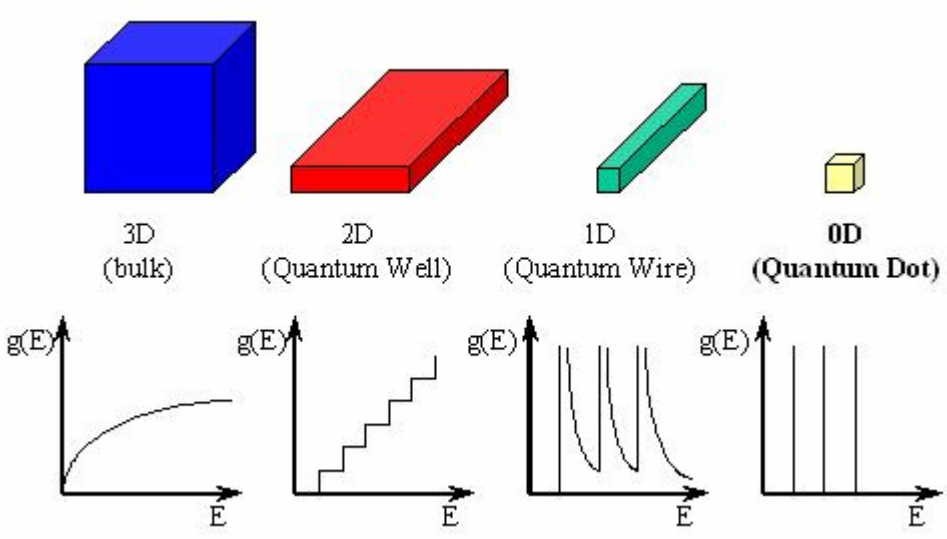

Figure 2. Quantum Confinement in Materials.[8]

The quantum confinement effect allows the tuning of absorption and emission wavelengths of QD's as a function of their size. This dependence can be illustrated by the equation describing the energy levels of the quantum dot system:[10]

$$E = E_g + \frac{(h/2\pi)^2}{2m_e}\left(\frac{\alpha_{n_e l_e}}{R}\right)^2 + \frac{(h/2\pi)^2}{2m_h}\left(\frac{\alpha_{n_h l_h}}{R}\right)^2 \qquad (1)$$

where, E_g is the band gap energy for the bulk semiconductor,

$\alpha_{n_e l_e}$ is the nth root of the l^{th} order Bessel function for the electron,

$\alpha_{n_h l_h}$ is the nth root of the l^{th} order Bessel function for the hole,

m_e and m_h are the effective masses of the electron and hole respectively,

R is the radius of the quantum dot.

The above equation is for a spherical quantum dot; in reality, quantum dots assume the shape of a polyhedron and are approximated to a spherical shape. So, the dependence of the energy of the quantum dot system on its radius can be approximated to $1/R^2$. The confinement effect also leads to altered emission lifetimes along with altered luminescence quantum efficiency.[10]

The energy transitions for the quantum dot that are shown in Figure 2 are ideal. The actual transitions are not discrete as a result of inhomogeneous and homogeneous broadening effects. Homogeneous broadening of the energy transition occurs as a result of phonon and other scattering effects.[10] Here, each transition for a given quantum dot size is broadened. Inhomogeneous broadening occurs because of the finite size distribution of the quantum dots resulting in a distribution of absorption/emission wavelengths. So in reality, the absorption/emission spectrum of a colloidal quantum dot sample assumes a complex structure as shown in Figure 3.

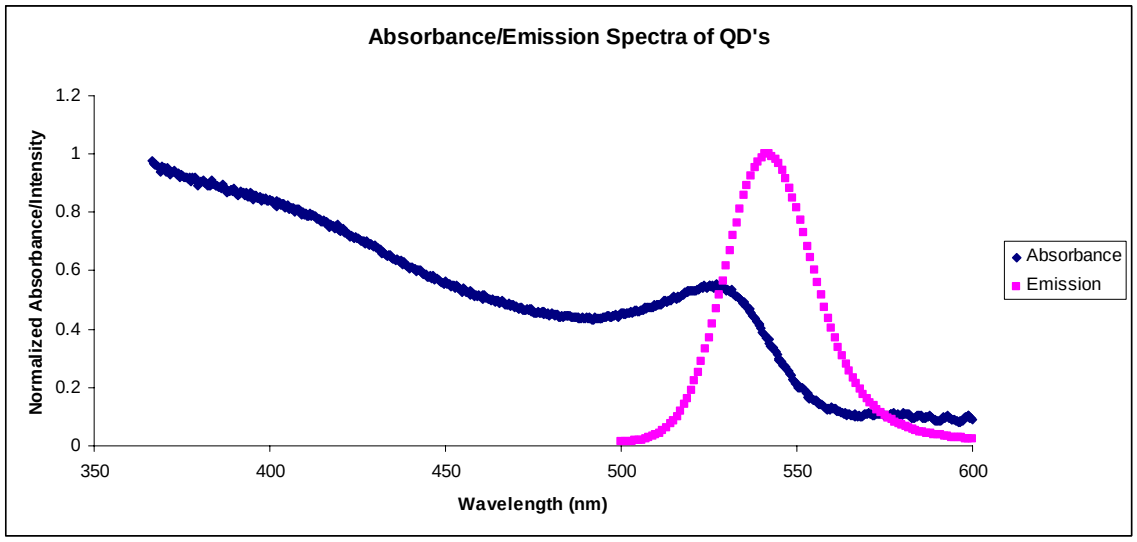

Figure 3. Absorbance & Emission Spectra of QD's.

Methods of QD Synthesis

There are two general classes of semiconductor QD's:

- *Epitaxial QD's*

  Self-assembled quantum dots nucleate under certain growth conditions during molecular beam epitaxy (MBE) and metallorganic vapor phase epitaxy (MOVPE). When a semiconductor material is grown on a substrate whose lattice structure is not matched to that of the material, the resulting strain produces islands of the semiconductor material nucleating on the surface. These islands can be subsequently buried to form the quantum dot.[12,13] The main limitations of this method are the cost of fabrication and the lack of control over positioning of individual dots.

- *Colloidal QD's*

In this method, QD's are grown in a solvent. The steps involved in the preparation of QD's are:

a) Nucleation

b) Growth

c) Quenching the growth

Colloidal quantum dots can be prepared either by aqueous chemistry or organometallic synthesis. The former employs low-temperature polar solvents like water or methanol where the synthesis temperature is limited by the boiling point of the solvent.[14] The latter synthesis method uses high-temperature, non-polar solvents such as trioctylphosphine oxide (TOPO).[15,16,17] The colloidal growth process is much cheaper and has the advantage of being able to occur at benchtop conditions.

This work involves preparation of Cadmium Selenide (CdSe) QD's by organometallic synthesis process. The CdSe QD's have an organic capping in the form of trioctylphosphine oxide (TOPO). The surface of the CdSe QD's has some crystal defects and is directly coupled to the TOPO. These characteristics reduce the quantum yield by allowing for non-radiative electron energy transitions at the surface. So, an inorganic shell of Zinc Sulfide (ZnS) is grown around the CdSe core to increase the quantum yield and luminescence.[18] Surrounding the CdSe core with a wide-bandgap semiconductor shell, like ZnS, reduces these non-radiative recombinations by passivating the CdSe surface and decoupling the CdSe core from the TOPO. This results

in brighter emission, provides long-term chemical stability, high quantum yield, and shorter emission lifetimes.[19, 20]

Advantages of QD's over Organic Fluorophores

Quantum dots have several advantages over organic dyes in imaging and sensing applications. They include:

a) Broad absorption band

b) Narrow and symmetric emission band

c) Size-tunable absorption and emission spectra

d) High levels of photostability

e) High quantum yield

a) Broad absorption band

Traditional organic dyes have the emission and absorption peaks close to each other. Also, they have narrow absorption bands leading to the need for a sharp cut-off filter in the detector path to separate the excitation and emission signals. In contrast, QD's have a broad absorption band over wavelengths shorter than the peak emission wavelength. A comparison between the absorption spectra of an organic dye, fluorescein isothiocyanate (FITC) and CdSe QD's is shown in Figure 4.[21]

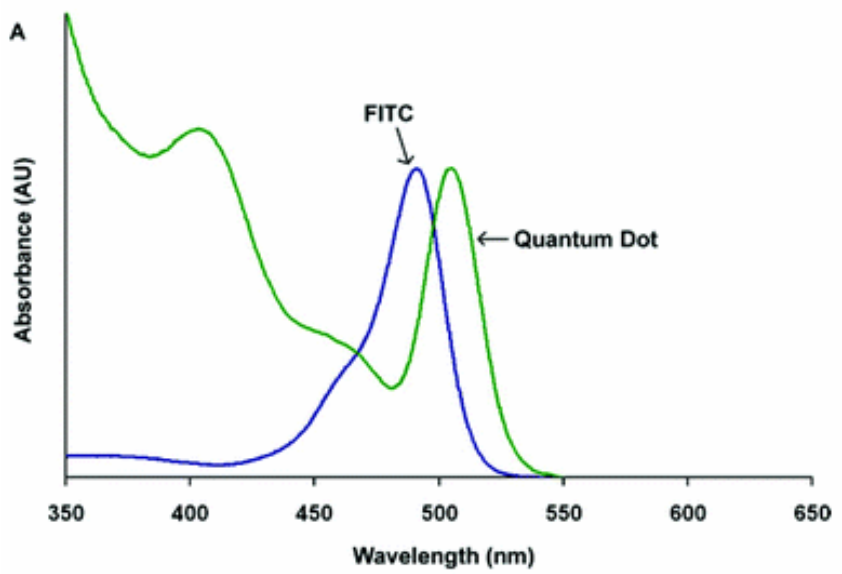

Figure 4. Comparison of Absorption Spectra between FITC and QD.[21]

Thus, the excitation and emission wavelengths can be spectrally separated and reduce the filtering requirements. Also, a single excitation source with a common long pass filter is sufficient to observe multiple QD's emitting in distinct wavelength ranges.[11,22]

b) Narrow and symmetric emission band

Another important property of QD's is their narrow and symmetric emission band.[11] The full width at half maximum (FWHM) of QD's is significantly less than most of the organic fluorophores thus making simultaneous detection of multiple-colored QD's possible. Figure 5 shows a comparison of emission spectra between CdSe QD's and the same organic dye, FITC mentioned above.[21]

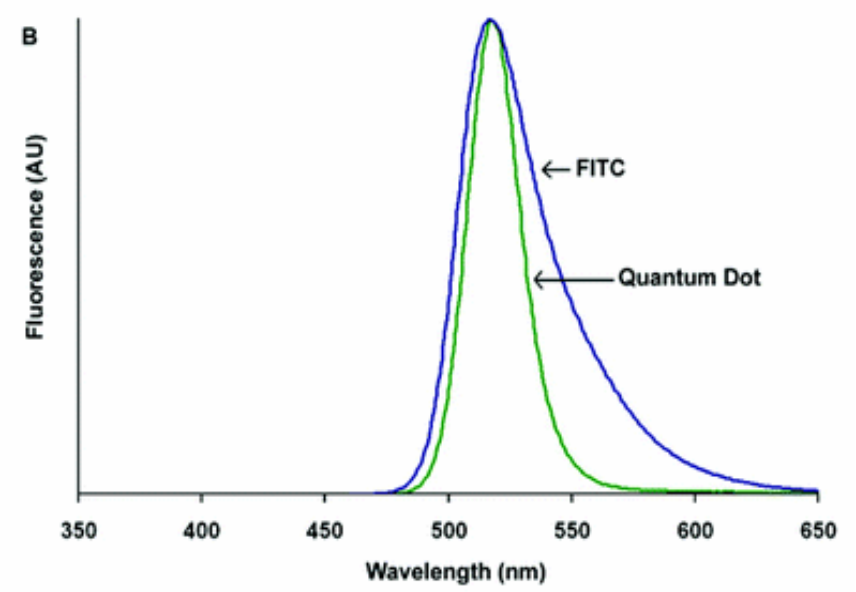

Figure 5. Comparison of Emission Spectra between FITC and QD.[21]

As seen from figures 4 and 5, the peak emission wavelength is shifted from the absorption peak and this shift in energy is called Stoke's shift. If taken from the first absorption peak, the Stoke's shift in QD's is much smaller than that of organic dyes. So, the use of a broad absorption band allows us to choose an excitation wavelength that produces a large effective Stoke's shift.

The very low spectral overlap of different QD's forms a very important part of this work. This concept, called spectral multiplexing, involves the simultaneous observation and spectral separation of a number of distinct QD populations. We specifically want to develop a system in which microspheres tagged with different-sized QD's can be functionalized to study bio-molecular interactions. These microspheric particles assume the spectral properties of the embedded quantum dots and so, can be excited by a single source to emit at different wavelengths. This will

lead to the detection of interactions of multiple bio-molecules, attached to these microspheres, simultaneously.[23-27]

c) Size-tunable absorption and emission spectra

The limiting of the exciton-Bohr radius of the bound electron-hole pairs leads to quantum confinement. As a result, their allowed energy states are also restricted as shown in Figure 2. This makes size the dominant factor in determining the absorption and emission spectra of QD's. The sizes of QD's can be controlled by the temperature of the synthesis process or by the type of ligand molecules used or by the duration for which the synthesis is run. Thus, through proper dimensional control, QD's can be produced to emit in a narrow color spectrum with minimal overlap between the full-width half maxima of the peak emissions at a single excitation wavelength,[10] which is not possible with organic fluorophores.

d) High levels of photostability

One of the main advantages of QD's is their resistance to photobleaching when compared to organic dyes. Wu et al.[28] studied the comparison of photostability between an organic dye (Alexa 488) and CdSe/ZnS QD's. In their work, they labeled nuclear antigens with QD-streptavidin emitting at 630 nm (red) and microtubules with Alexa 488, conjugated with IgG, having an emission peak at 488 nm (green). The specimens were continuously illuminated for 3 minutes with a 100 W mercury lamp. They could observe that the labeling signals of Alexa 488 faded completely within 2 minutes while the QD's did not show any photobleaching.

They repeated the same procedure with a reversal of the labels on nuclear antigens and microtubules where again, the Alexa 488 underwent significant photobleaching within the first 2 minutes of illumination while the QD's had their emission intensity almost constant throughout the observation period. This shows that QD's are ideal for biomedical applications where the target samples have to be tracked continuously for a long time.

e) High quantum yield

One main problem in CdSe QD's is their existent surface defects which lead to alternate decay paths reducing the overall quantum yield, defined as the ratio of emitted to absorbed photons. One way to overcome this problem is to grow a shell of a few atomic layers of a material with a larger band gap on top of the nanocrystal core. It has been found that the shells increase the quantum yield of the dots close to 90% in some cases. The core-shell structure also enhances the photostability of the QD's by several orders of magnitude relative to conventional dyes.

It should also be noted that QD's possess a long fluorescence lifetime[19] which enables the use of time-gated detection[29] to separate their signal from that of shorter lived species. This can be important in biomedical applications as the background autofluorescence may be temporally eliminated.

One of the major problems in using CdSe or CdSe/ZnS QD's in biomedical applications is their possible cytotoxicity. The cadmium and zinc ions released are biologically toxic and so, cannot be used for *in vivo* applications. Various research

groups[30,31] are coating the surfaces of QD's with different materials to probe their usage in biological samples but none of the methods have led to a decisive conclusion.

TOTAL INTERNAL REFLECTION MICROSCOPY

Total Internal Reflection Microscopy (TIRM) is an experimental technique used to monitor the interactions between colloidal particles and a surface. The instantaneous separation distance between the particles and the surface is determined by monitoring the intensity of light that is scattered by the particles. This scattered light is generated by evanescent waves interacting with the levitated colloidal particles. The property of the evanescent wave to exponentially decay normal to the surface results in scattered intensities expressed as a function of the particle-surface separation distances. Most importantly, this exponential decay contributes to the high sensitivity of TIRM where separation distances as small as 1 nm can be detected.

We can use this height information to determine the potential energy of interaction between the particles and the surface using the equilibrium distribution of separations sampled by the Brownian motion of the particles at different time intervals.[1]

Evanescent Waves

As the name suggests, the TIRM system relies on the principle of total internal reflection. According to Snell's law,

$$n_1 \sin\theta_1 = n_2 \sin\theta_2 \qquad (2)$$

where n_1 and n_2 are the refractive indices of the incident and refractive media respectively, θ_1 and θ_2 are the angles of incident and refraction respectively. When light is incident on a medium of lower refractive index, both reflection and refraction of the

incident wave occur. The critical angle is the angle of incidence above which total internal reflection (TIR) occurs and at this angle of incidence, the angle of refraction is 90^0. During TIR, all of the light is observed to be reflected back into the incident medium. The critical angle is given by,

$$\theta_c = \sin^{-1}\left(\frac{n_2}{n_1}\right) \tag{3}$$

During TIR, evanescent waves penetrate into the lower index medium and their intensity decreases exponentially normal to the interface at which they are formed. The relationship is given by,[1]

$$I(h) = I_0 \cdot \exp(-\beta h) \tag{4}$$

where *I(h)* is the intensity of the evanescent wave at height *h*,

I_0 is the intensity of the evanescent wave at the surface (*h*=0) and,

β^{-1} is the evanescent wave decay length from the surface.

Figure 6 explains the evanescent wave phenomena.[32]

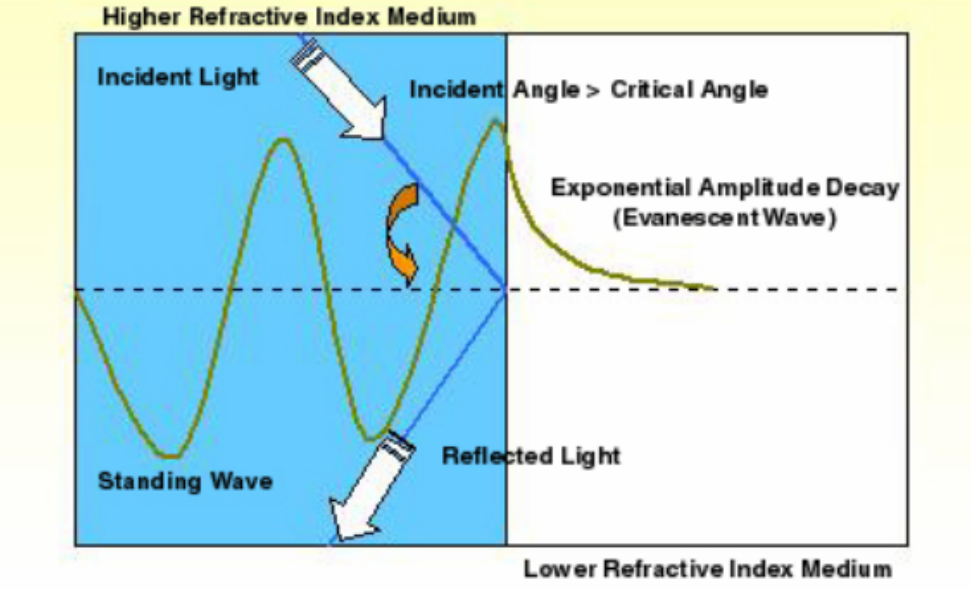

Figure 6. Evanescent Wave Generation.[32]

The scattering intensity of a particle decays with the same dependence on distance from the boundary as the intensity of the evanescent wave itself.[1] Thus, we can use equation 4 to calculate the scattered intensity of a particle as well. Here, I_0 is the scattered intensity when the particle is at the surface (h=0) and the decay length, β^{-1} is given by,[2]

$$\beta = \frac{4\pi}{\lambda}\sqrt{(n_1.\sin\theta)^2 - n_2^2} \qquad (5)$$

The penetration depth of the evanescent wave from the surface is approximately 87 nm for our system. Penetration depth is defined as the height from the surface at which the intensity of the evanescent wave decays to 1/e of the incident intensity. The value of I_0 is constant for each particle and is very sensitive to the particle size.[3]

Problems arising from particle polydispersity in our applications will be discussed in detail in later sections.

Working of TIRM

The TIRM system involves suspending microspheres in an aqueous solution on top of a glass slide. The motion of the levitated particles is caused by their Brownian motion and the important forces acting on the particles which maintain them at a levitated state are: [1]

a) Force due to the interaction between overlapping double layers on the particles and surface,

b) Gravitation due to the buoyant weight of the particle and,

c) Van der Waals attraction between the particles and surface.

There is a particular separation at which the repulsive and attractive forces are exactly balanced for the microspheres. Although this distance corresponds to a mechanical equilibrium condition, the microspheres are not stationary.[1] Instead, they sample the elevations above and below this equilibrium separation distance because of Brownian motion. The locations having high potential energy (PE) are sampled less frequently than the ones having low PE. Figure 7 shows a single microsphere levitated at a distance h from the glass surface.[1]

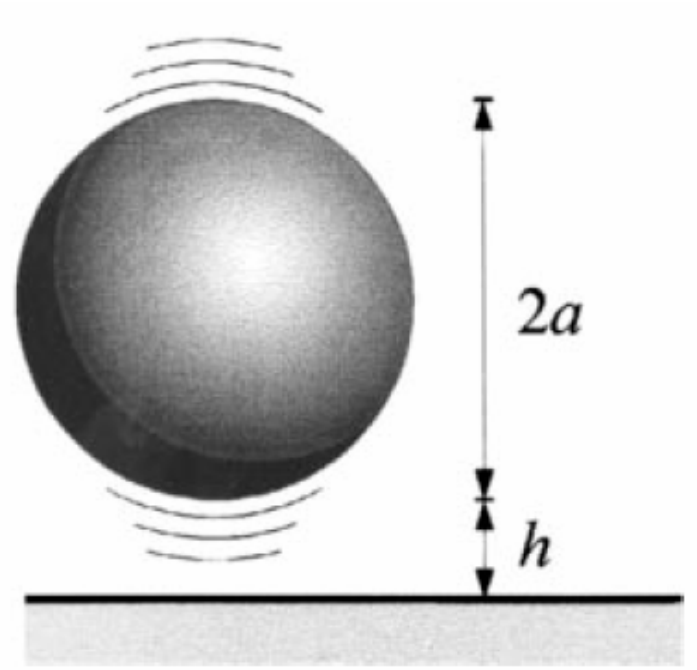

Figure 7. Brownian Motion of a Single Microsphere.[1] Reprinted from Advances in Colloid and Interface Science, 82, Prieve, D.C., Measurement with TIRM, 93-125, 1999, with permission from Elsevier.

In our TIRM system, incident light is generated from an Ar-ion laser and is directed at an angle greater than the critical angle so that an evanescent wave is produced at the interface between the glass slide and the aqueous solution. As shown in Figure 8, the levitating microspheres scatter the light and the scattered intensity follows the same exponential relation as the evanescent wave with the distance from the surface. As a result, we can use the scattered intensity from the particles to directly measure the instantaneous separation between the microspheres and the glass slide by using equations 4 and 5.

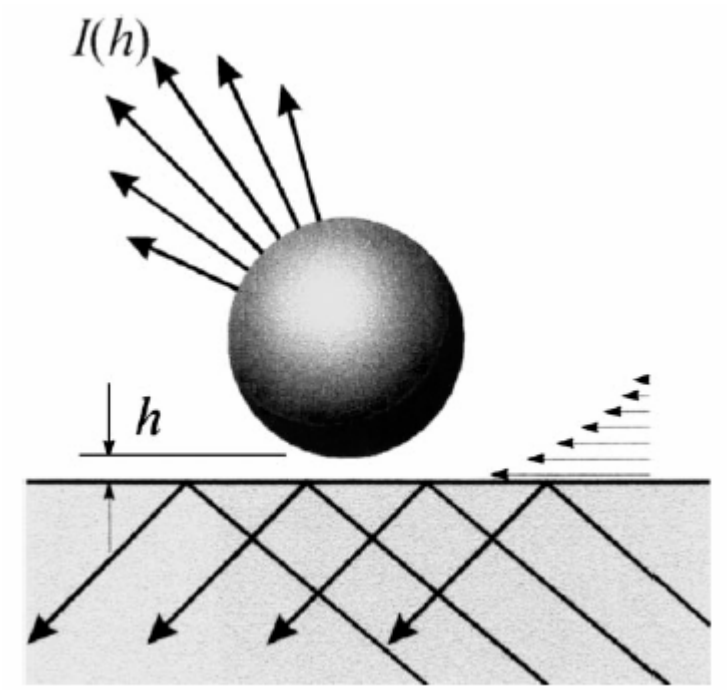

Figure 8. Basic Set-up of the TIRM System with a Single Particle.[1] Reprinted from Advances in Colloid and Interface Science, 82, Prieve, D.C., Measurement with TIRM, 93-125, 1999, with permission from Elsevier.

Chew et al.[33] solved the scattering problem for a $1\,\mu$m sphere excited by an evanescent wave using Mie theory. They concluded that the intensity of scattering is a complicated function of polarization and direction of the evanescent wave, involving multiple peaks and valleys. On the other hand, TIRM integrates the scattered intensity over a cone of solid angle corresponding to the numerical aperture of the microscope objective lens. They also found that the intensity of scattering in any direction decays exponentially with elevation of the sphere above the surface thus making the integrated scattering intensity sensed by the CCD also decay exponentially with elevation.

Measurement of Potential Energy Profile

The total potential energy (PE) of a particle levitated above a surface can be found by adding the gravitational, electrostatic, and van der Waals forces. TIRM is a technique which indirectly measures the instantaneous separations between particles and the surface from the scattered intensities. The probability of finding a single microsphere at a particular height depends on the PE of the particle at that height. Locations having lower PE correspond to higher frequency of sampling and vice versa. This relation is given by Boltzmann's equation:[1]

$$p(h) = A \cdot \exp\left(-\frac{\phi(h)}{k_B T} \right) \tag{6}$$

where *p(h)*is the probability of finding the sphere at height h, k_B is Boltzmann's constant, *A* is a normalization constant, $k_B T$ is the thermal energy and $\phi(h)$ represents the PE of the particle at height *h*.

By measuring the number of times a particle samples each height during an experiment, a histogram of the particle height, *n(h)* can be determined. A large number of observations are used to make sure there is sufficient statistical sampling. Thus, *n(h)* can be considered a good approximation of the probability density of heights, *p(h)* in the calculation of PE.[1]

Thus, the PE relative to the PE at a reference height is given by,[2]

$$\frac{\varphi(h) - \varphi(h_{ref})}{k_B T} = \ln\left[\frac{n(h_{ref})}{n(h)} \right] \tag{7}$$

where h_{ref} is the reference height which is normally h_m, the most probable height sampled in *n(h)*.

Diffusing Colloidal Probe Microscopy (DCPM)

The above measurement is for single-particle TIRM. In the case of ensemble TIRM employing multiple particles, a technique which combines TIRM and video microscopy is used. Using this new technique known as Diffusing Colloidal Probe Microscopy (DCPM), the height fluctuations of multiple individual particles are tracked as a function of time, and can be averaged together to produce an ensemble average histogram. This can give us the ensemble particle-surface interactions averaged over all particles and all heights sampled by the particles. This has been explained in detail by Wu et al.[2]

The DCPM technique has been shown to exhibit sensitivity to potentials on the order of k_BT. An example of a single-particle PE profile obtained from a histogram is shown below in Figure 9.[1]

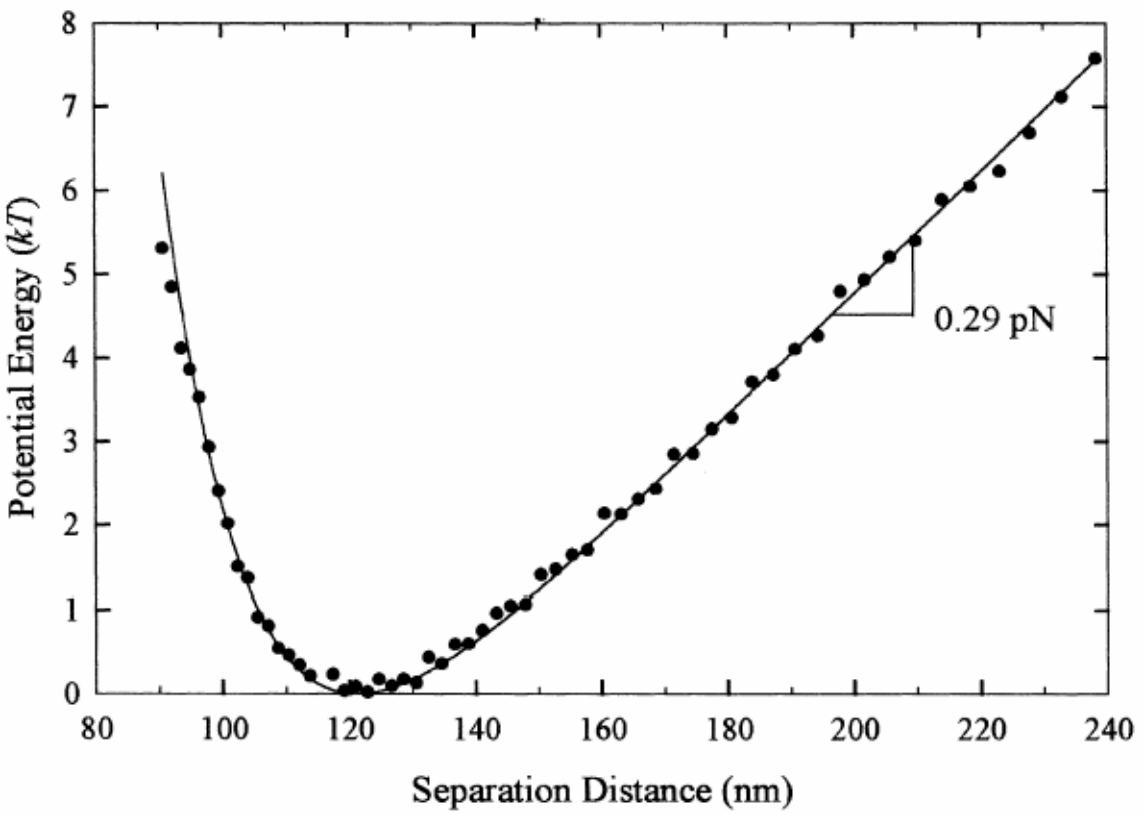

Figure 9. Single Particle Potential Energy Profile.[1] Reprinted from Advances in Colloid and Interface Science, 82, Prieve, D.C., Measurement with TIRM, 93-125, 1999, with permission from Elsevier.

The above profile corresponds to a situation when only gravity and double-layer repulsion are present. When the microsphere is far from the surface, it is outside the range of interactions with the surface leaving gravity as the dominant force. This is the part of the profile where PE increases linearly with the separation distance. When the sphere is closer to the surface, it experiences double-layer repulsion which causes the PE to increase with decrease in separation.[1]

From the relation between probability density profile *p(h)* and PE $\phi(h)$ as shown in equation 6, the lower the particle's PE at a particular location, higher the probability to find it at that location. Thus the most probable location corresponds to the bottom of the PE well where gravity and double-layer repulsion are equal and cancel each other's effects.[1]

DCPM Setup

The experimental set-up of the DCPM system is shown in Figure 10.[2]

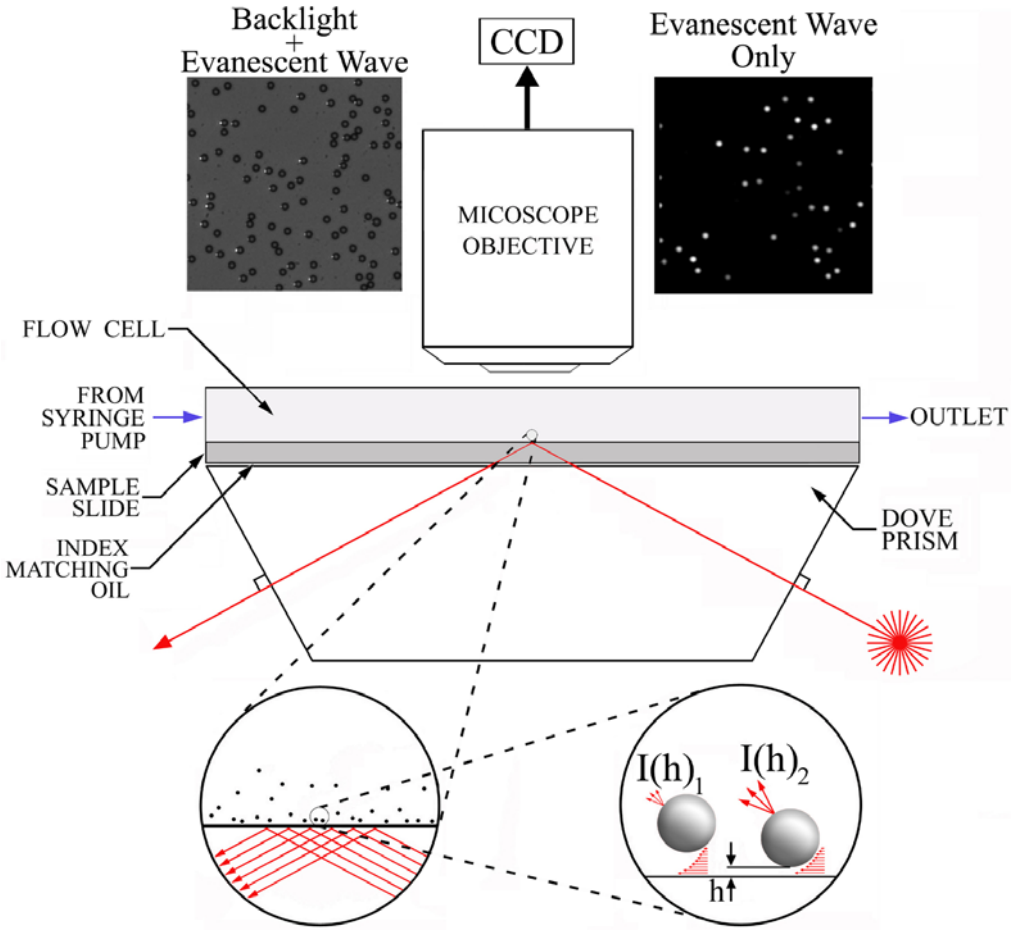

Figure 10. DCPM System Set-up.[2]

An optical microscope and a CCD camera are used together to dynamically track and monitor the scattering from ensembles of particles undergoing Brownian motion. The sample containing the particles in an aqueous solution is placed in the flow cell which is optically coupled to the dove prism using index-matching oil. The evanescent wave used in the system is generated using a single line Ar-ion laser at 488 nm.

The insets at the top of Figure 10 are the CCD images from top view of levitated particles scattering the evanescent wave. The left inset shows the scattered light as white spots with the transmitted light illuminating the particles shown as dark rings. The right inset shows the evanescent wave scattering without the backlight thus showing only the scattered light from the particles. The increase in brightness of the scattered light corresponds to particles being closer to the surface. The bottom insets in Figure 10 show a schematic representation of levitated particles scattering evanescent wave with intensity $I(h)$, as a function of particle-surface separation, h. The video microscopy system monitors this over a long period of time thus accumulating enough scattering data to plot the potential energy profile of particle ensembles.

SIGNIFICANCE

DCPM IN BIOMEDICAL RESEARCH

Techniques such as Surface Force Apparatus (SFA), Optical Trapping and Atomic Force Microscopy (AFM) are well-suited to measuring the equilibrium interaction of two bodies. However, they are limited in force resolution due to the application of a restoring or trapping force by the experimental system. Since colloidal particles undergo Brownian motion and the particle-surface distance continuously fluctuates,[1] characterization of Brownian motion presents a high resolution technique for characterizing particle-surface interactions and this is accomplished by our DCPM system.[2] Colloidal particles have been investigated for bio-molecular tagging by various research groups.[23-27] So, DCPM can potentially be a groundbreaking technique monitoring interactions between bio-molecules with kT-level energy resolution. The technique has been shown to exhibit force sensitivity two orders of magnitude more than atomic force microscopy (AFM) and Optical trapping.

Even though this work does not focus on bio-molecules *per se*, it develops a tool to monitor bio-molecular interactions simultaneously and accurately. The force resolution of DCPM is in the order of kT as seen from equation 6. This combined with DCPM's excellent spatial resolution makes it an ideal technique to monitor functionalized particle-surface interactions. Surface Plasmon Resonance (SPR) is another technique which can be used to quantify the Brownian motion of particles but it suffers from a poor lateral resolution which is in the range of microns.[34] Many of the

specific and non-specific interactions of bio-molecules have been shown to take place in the first few nanometers and the ability of DCPM to track interactions taking place at small distances sets it apart from other contemporary techniques. We believe that the quantitative observations of interactions using this method will lead to significant advances in the field of bio-molecular dynamics.

NEED FOR SPECTRAL MULTIPLEXING

This work focuses on developing a tool which can be used in the detection and analysis of individual bio-molecular interactions in a complex mixture simultaneously. For this, we employ spectral multiplexing where functionalized microspheres are labeled with quantum dots of different emission wavelengths and detected simultaneously with a single excitation source. The most important advantage of spectral multiplexing is the ability to perform parallel and high-throughput analysis of a large group of bio-molecules.

Various research groups have recognized the importance of spectral multiplexing and have used it for different applications.[23-27,35] Han et al. designed a DNA hybridization system using oligonucleotides probes and QD-tagged microspheres.[23] Meissner et al. investigated a fluid-based DNA microarray system with quantum dots embedded in polystyrene microspheres.[27] Diaz et al. have developed a high-throughput fungal identification system for a particular species.[36]

Quantum Dots in Multiplexing

Quantum dots are ideal luminophores for spectral multiplexing because their luminescence emission wavelength can be continuously tuned by changing the particle

size, and a single wavelength can be used for simultaneous excitation of different-sized QD's.[9,11] In addition, the CdSe/ZnS QD's are highly photostable and have narrow, symmetrical emission peaks. These properties allow us to severely reduce spectral overlaps resulting in highly efficient spectral read-outs. We have used hydrophobic QD's in our experiments; methods for rendering the QD's water-soluble for use as biological labels have been reported by various authors.[37-41]

NEED FOR LUMINESCENCE IN DCPM

The exponential decay of the evanescent wave normal to the surface results in scattered intensities that vary with particle-surface separation distance. This distance is also a function of the particle size as particles of different sizes have different scattering intensities despite being located the same distance from the surface.[3] Polydispersity, which is present in all particle samples, is one of the major contributing error factors in calculations of potential energy from intensity distributions.

To look at the effects of polydispersity, the ionic strength of the aqueous solution in which the particles are suspended is modified so that the particles can stick to the surface. In these experiments, the so-called stuck intensity of the colloidal particles exhibit intensities that vary up to 10 times.[3] If the particles are polydisperse in multiple-particle DCPM, the assumption of a constant I_0 (from equation 4) for all particles for an experiment will result in incorrect estimations of the heights of particles from surface. This will in turn result in erroneous calculations of the potential energies of the particle-surface interactions. An early investigation in this regard can be seen in the work by Allen.[3]

Also, the scattering characteristics can be different in a particle ensemble if the particles are affected by non-uniformities in their structure. This will again lead to erroneous mapping of PE profiles of particle-surface interactions.

To mitigate the above effects, we use luminescence as the mode of detection of the particle height from surface. We hypothesize that luminescence has reduced dependence on particle non-uniformities and is less sensitive to small size variations in particles. According to this assumption, the measured I_0 for a large particle-ensemble is constant for all particles thereby reducing the probability of error during monitoring of particle-surface interactions.

Another important advantage in using luminescence is the ability to perform spectral multiplexing to simultaneously monitor multiple analytes. If different bio-molecules are attached to the surface of microspheres labeled with different-sized quantum dots, we can simultaneously monitor the interactions between the bio-molecules and the surface, with the surface being coated with another bio-molecule. Even though this work does not explicitly involve monitoring of bio-molecular interactions, we anticipate this will be a very good application of the DCPM-quantum dot technique given the DCPM system's force sensitivity that matches the requirements for analysis of bio-molecular interactions, and the quantum dots' optical properties.

EXPERIMENTAL DETAILS

SYNTHESIS OF QUANTUM DOTS

Materials

Trioctylphosphine oxide (TOPO, 99% pure), cadmium oxide powder, selenium powder, and trioctylphosphine (TOP, 90% pure) were purchased through Sigma-Aldrich, St.Louis, Missouri. Tetradecylphosphonic acid (TDPA, 98% pure) was purchased through Alfa Aesar, Ward Hill, MA. Methanol, ethanol and toluene were purchased from VWR International Inc., West Chester, PA. Hexamethyldisilathiane and dimethylzinc required for the ZnS capping of CdSe quantum dots were purchased through Sigma-Aldrich as well. Syringes and needles of various specifications were purchased from VWR.

Set Up

Our home-made reactor for the organometallic synthesis of CdSe/ZnS quantum dots is shown in Figure 11. A stirrer was connected to a stir bar made of aluminium to stir the reaction sample. A heating mantle filled with a bismuth alloy served as the heat bath. A temperature probe and controller were used to monitor the reaction temperature. A separate stir plate was used to stir the TOP-Se mixture. An Argon bubbler was used to make sure that there was constant argon flow into the reaction glassware.

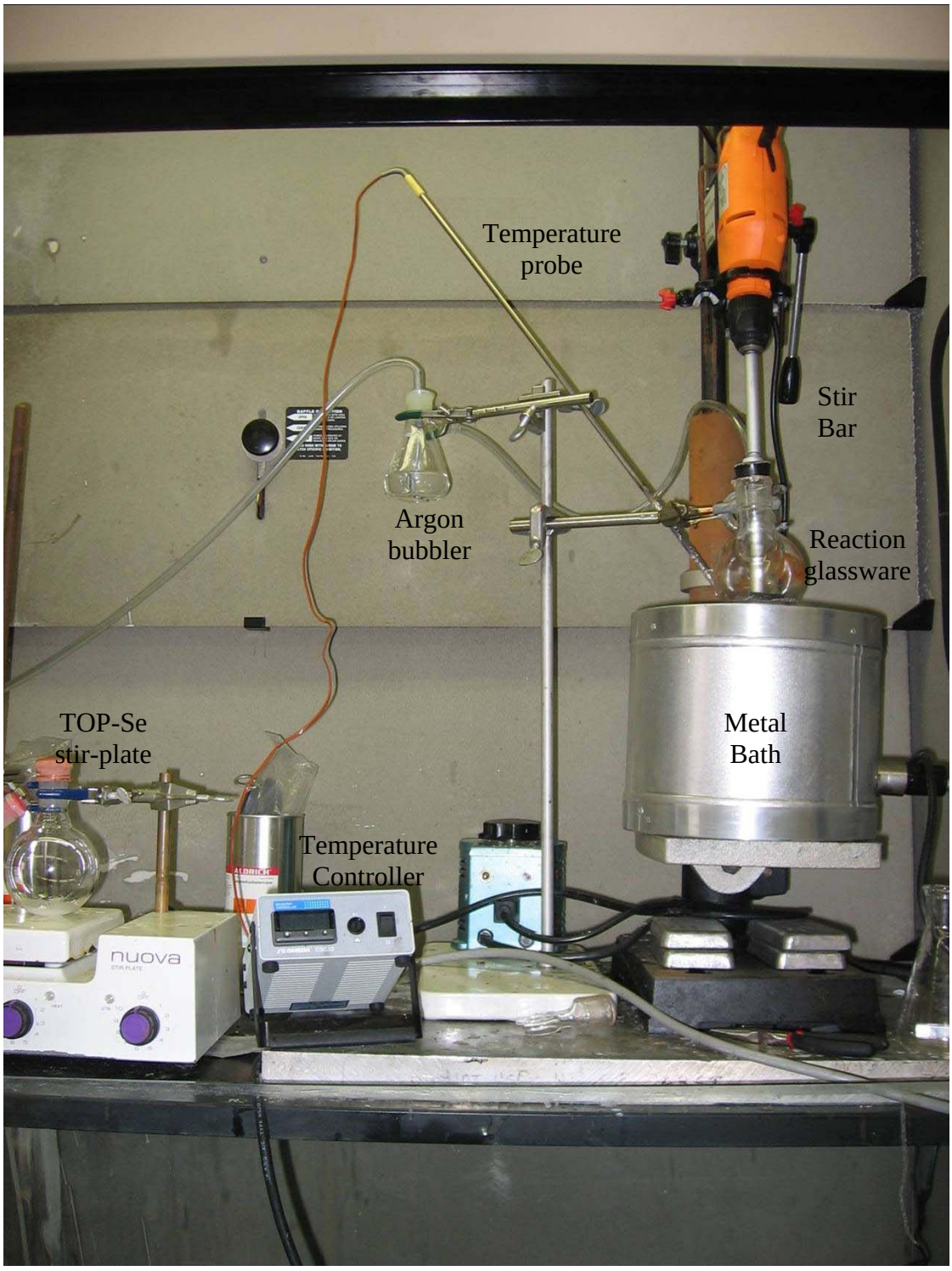

Figure 11. Metal Bath Reactor to Perform Organometallic Synthesis of QD's.

Methods

0.0514 g of Cadmium oxide (CdO) was heated in argon atmosphere in 3.7768 g of trioctylphosphine oxide (TOPO) and 0.0567 g of tetradecylphosphonic acid (TDPA) at 340°C until the color changed from dark brown to nearly colorless. 0.0411 g of selenium was stirred in 2.4 ml of trioctylphosphine (TOP) under argon at the same time until the selenium dissolved. The temperature of the Cd-TOPO solution was reduced to 270°C once the solution was nearly colorless.[18]

At this point, the selenium solution was injected into the cadmium precursor and the reaction began immediately and aliquots were removed at various time intervals depending on the required size of the QD's. These samples contained different sized CdSe quantum dots according to their growth time in solution and as a result, QD's of different emission maxima were produced. The quantum dots were then washed multiple times with methanol and toluene, and then stored in toluene. The sample of quantum dots obtained from the reaction typically looks like those shown in Figure 12 (taken from Meissner lab) when illuminated by UV light.[42]

Figure 12. QD's Suspended in Toluene.[42]

Capping of the CdSe QD's with ZnS structure was done after initial CdSe core particle growth. After the growth time required for QD's of a particular emission wavelength, the temperature was dropped to approximately 200°C and then, a ZnS precursor solution, consisting of 6.4 ml dimethyl zinc and 1.6 ml hexamethyldisilathiane maintained in argon environment, was injected over a period of one to two minutes to allow for formation of the shell structure. After allowing 1 hour for the shell formation, the temperature was reduced to 100°C to anneal the particles. Annealing was performed for 30 minutes, and then the CdSe/ZnS particles were quenched in methanol and purified according to the procedures described earlier for CdSe/TOPO.

INCORPORATION OF QUANTUM DOTS INTO POLYSTYRENE MICROSPHERES

CdSe/ZnS quantum dots were embedded inside polystyrene microspheres using a previously reported procedure.[23] 4 μm polystyrene microspheres (4.1%, purchased from Interfacial Dynamics Corporation, Portland, Oregon) were purified repeatedly with ethanol and butanol. 3 mL of butanol/ chloroform (95-5 %) mixture was added to the microsphere sample and this mixture was stirred gently for 24 hours to facilitate swelling of the microspheres.

A sample of CdSe/ZnS quantum dots suspended in toluene was cleaned with methanol and then dispersed in chloroform. This quantum dot sample was added to the solution consisting of the swollen polystyrene microspheres and the mixture was stirred gently for 48 hours. This resulted in the incorporation of quantum dots inside the

microspheres. The diffusion of quantum dots was limited to the space near the surface of the microspheres.

After incorporation of quantum dots, the microspheres were dried in a nitrogen atmosphere in order to push the chloroform out of the microspheres. This resulted in the shrinking of the microspheres to their original sizes leaving the QD's trapped inside the polystyrene structure. These microspheres were subsequently washed with butanol and ethanol and then finally suspended in DI water. The procedure was repeated for different sized QD's to obtain microspheres which appeared to have different colored "rings".

DIFFUSING COLLOIDAL PROBE MICROSCOPY

The experimental setup of the DCPM system is fully explained by Wu et al.[2,43] Microscope glass slides were used as surfaces in all the experiments covered by this work. The surfaces of the cover glass were initially washed for 30 minutes in Nochromix followed by rinsing with double deionized water (DDI) and drying with high purity nitrogen. A 10mm ID x 12 mm OD Viton O-ring (McMaster Carr, Los Angeles, CA) was attached to the cover glass using polydimethyl siloxane (PDMS), for use as spacers for the sedimentation cell.

Fig 6 shows a schematic representation of an optical microscope (Axioplan 2, Zeiss, Germany) and CCD camera setup for dynamically tracking and monitoring evanescent wave scattering and luminescence from particle ensembles. An O-ring/cover glass batch sedimentation cell is optically coupled to a 68° dove prism using index matching oil with index of refraction, n=1.515. The prism is mounted on a three point leveling stage. Depending on the experiment, we used 63X or 100X objective in

conjunction with a 12 bit CCD camera (ORCA-ER, Hamamatsu, Japan) operated with 8x binning to produce a capture rate of 42 frames/sec with 672 x 512 resolution (pixel=304nm and , 204 x 155 μm^2 image size for 40X objective). The evanescent wave was generated using a 150 mW, 488 nm Argon Ion laser to produce an evanescent wave decay length of 88 nm (n_g=1.515, n_w=1.333).

Image analysis algorithms coded in FORTRAN were used to track the lateral motion of the particle and also, to integrate the evanescent wave scattering intensity for each particle. The scattering intensities of stuck particle ensembles were measured and averaged for a short period of time so that an absolute value can be established for the scattering intensity of the levitated particle. Standard video microscopy algorithms were used to locate and track centers of the evanescent wave scattering signal on each particle.[44] The total scattering intensity from each particle was calculated by integrating all pixels within a specified radius of the scattering signal center pixel. All image analysis was performed using PCs and multi-page TIFF files.

RESULTS AND DISCUSSION

QUANTUM DOTS SYNTHESIS

The organometallic synthesis process resulted in three samples of quantum dots. The CdSe quantum dot samples were obtained by removing aliquots from the reaction sample at 4, 16 and 60 minute time intervals. Each of these samples was then capped with a ZnS layer. The various samples contained different sized nanoparticles according to the growth time in solution and hence, different emission peaks were achieved, as shown in Figure 13. The intensities have been normalized in the figure.

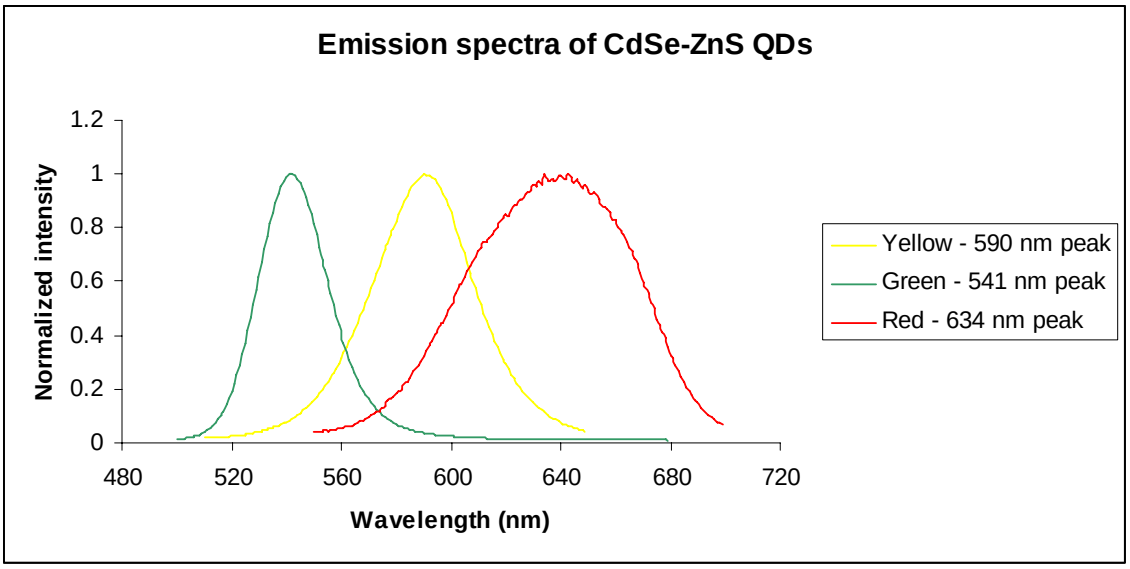

Figure 13. Photoluminescence Spectra of CdSe Quantum Dots.

In order to have minimal spectral overlap between the emission spectra of the QD's, only three samples were pulled out during the synthesis process. Due to their

broad absorption spectra, all three QD samples were illuminated by the same excitation source with peak intensity at 488 nm. This will enable us to monitor colloidal particles tagged by these quantum dots effectively in our DCPM system.

INCORPORATION OF QUANTUM DOTS INTO POLYSTYRENE MICROSPHERES

Figure 14 shows an image of 4 μm polystyrene microspheres, with 590 nm QD's embedded in them and observed with a confocal microscope. The particles were excited by a single line Ar-ion laser at 488 nm. A long pass filter of 505 nm was employed to block the excitation wavelength and allow detection of the QD luminescence. This image shows an equatorial cross-section of the QD-tagged microspheres.

As shown in the figure, the quantum dots are of uniform concentration near the surface of the microspheres. We can observe from the image that the three particles seem to have layers of quantum dots of uniform thickness.

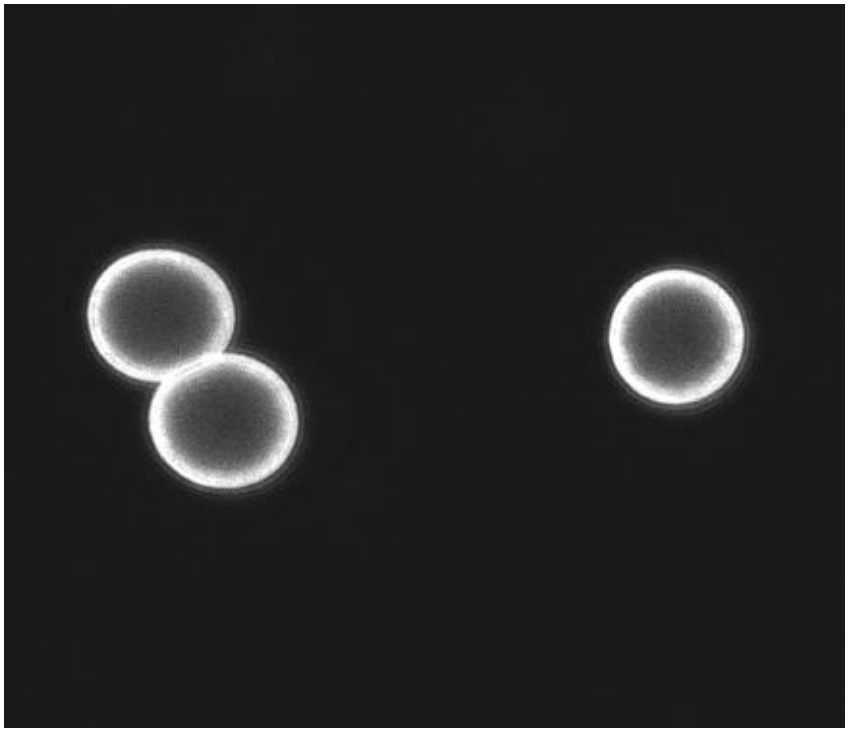

Figure 14. Confocal Image of 590 nm QD's Incorporated into 4 μm Polystyrene Microspheres.

The thickness of the layer, after performing digital processing of the image, seems to be ~150-200 nm. Since this is less than the resolution of our microscope (~250 nm), we are not yet sure whether the QD's are inside the microspheres or stuck on the outer surface. TEM measurements in the future must lead to a definitive conclusion. Han et al. report that the QD's are inside the microspheres with a similar QD incorporation procedure.[23]

DCPM OF QUANTUM DOT-EMBEDDED MICROSPHERES

We performed a DCPM experiment with the QD-embedded microsphere stuck to the surface to capture the luminescence due to the particle. This is shown in Figure 15.

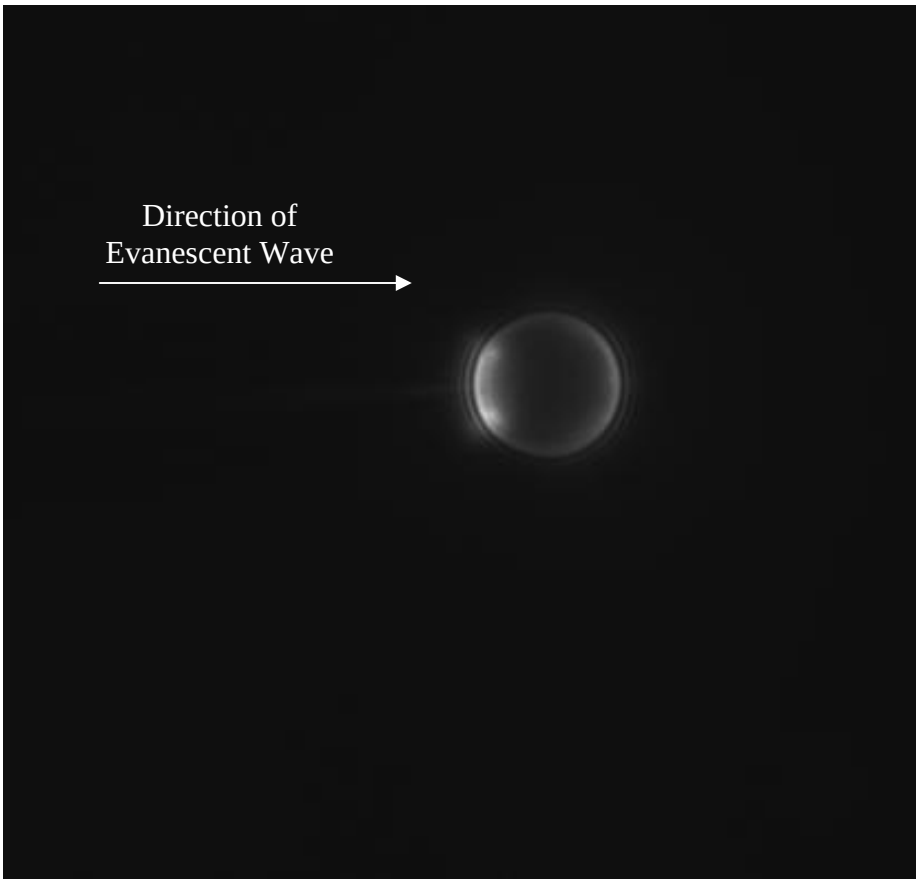

Figure 15. QD-tagged Microsphere Stuck to the Surface and Excited by Evanescent Wave in the DCPM System.

The above image was captured with a 100X objective. A 150 mW 488 nm Ar-ion laser source was used to generate the evanescent wave to excite the quantum dots inside the microspheres. The capture time was 28 ms and a long pass filter with 505 nm cut-off was placed for emission to block the scattering due to the particle.

As shown in the figure, the direction of the evanescent wave is from left to right and the QD's luminesce isotropically upon excitation with evanescent waves. The peak luminescence is on the left side of the QD-tagged microsphere. In the case of scattering

in DCPM, the evanescent wave would exit at the opposite side of its entrance to the microsphere (in this case, it would be on the right). This is clearly illustrated by Figure 8. We see that the introduction of luminescence due to QD's have resulted in a highly modified system with the pattern of QD emission being significantly different from scattering from microspheres. More studies in the future should help us understand the origin of this pattern better and also would enable us to exploit the advantages of the luminescence introduced DCPM system.

Now that I_0 has been determined in the previous experiment, we can calculate the instantaneous separation distances from the observations of a DCPM experiment with luminescent QD-embedded microspheres. Figure 16 shows an image of QD-embedded microspheres luminescing when excited by evanescent waves with peak intensity at 488 nm. The laser power was the same as the previous experiment at 150 mW. A 63X objective was used in this experiment.

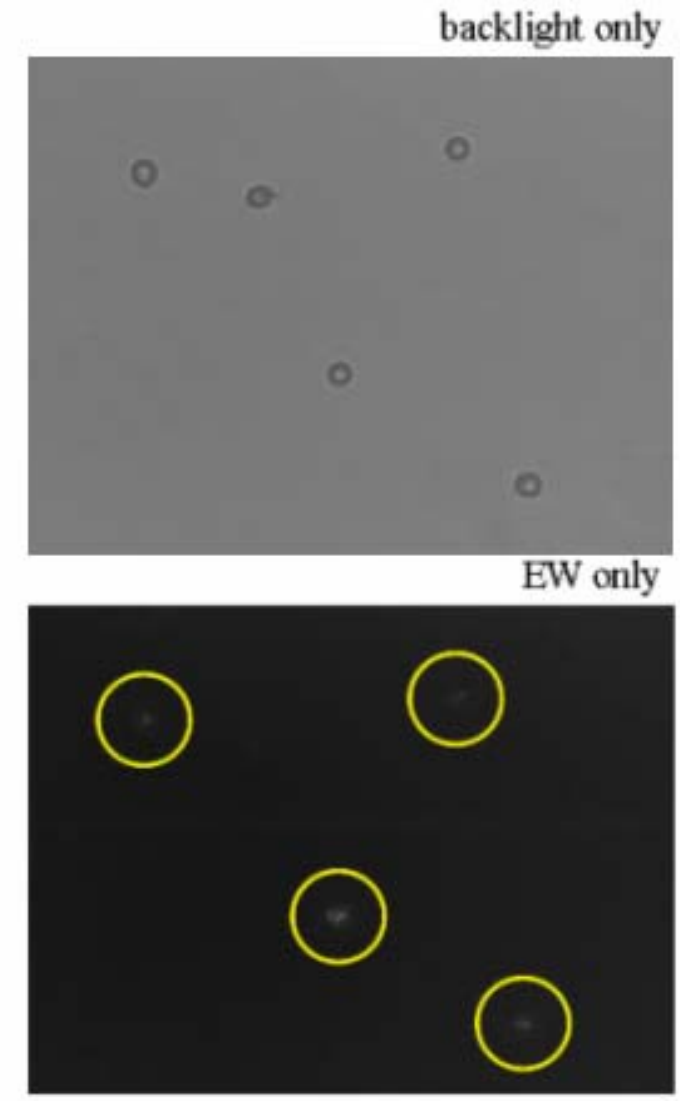

Figure 16. DCPM Image Showing Luminescence Due to 590 nm QD's Embedded in 4 μm Polystyrene Microspheres.

The top half of the figure is an image captured with the backlight switched on. The clear outline of the microspheres can be seen here. The bottom image shows luminescence due to QD's excited by evanescent waves. The luminescent microspheres have been marked by yellow circles for easy viewing. It should be noted that there is one

particle that is seen when the backlight is present but not luminescent when the backlight is switched off signifying that it does not have sufficient amount of QD's embedded in it to be observed or the particle is outside the decay length of the evanescent wave.

The experiment collected 80,000 frames at the rate of 43 frames/sec (approximately 31 minutes) to build up enough intensity values and hence separation distances.

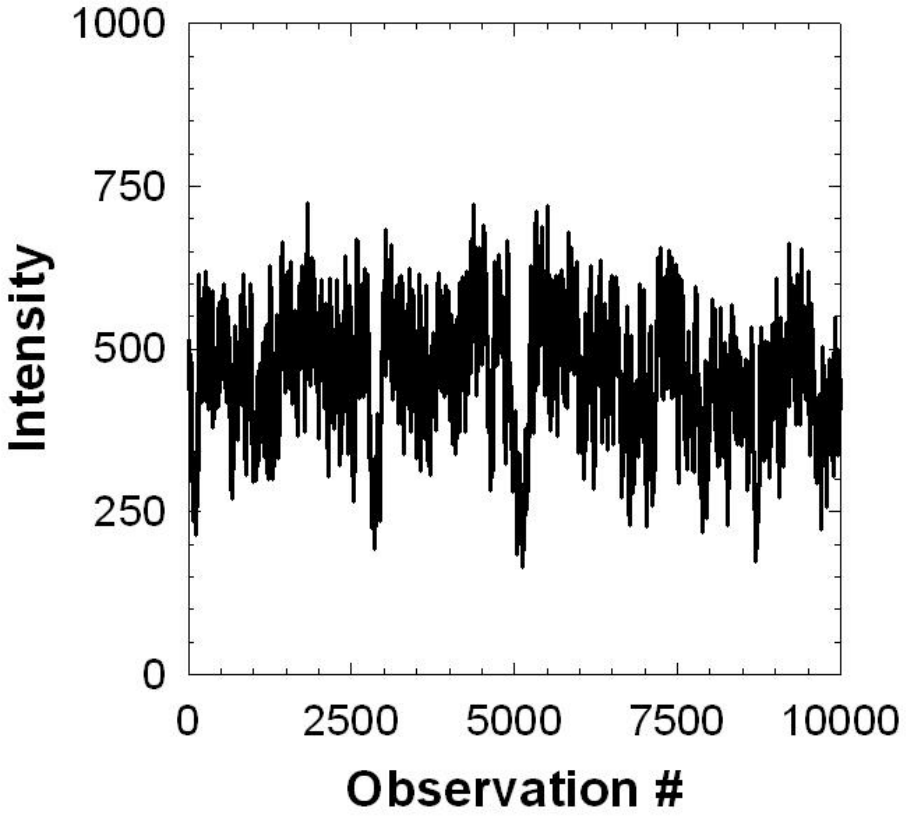

Figure 17. Fluctuation in Evanescent Wave Scattering Intensity from Particle Over an Interval of Time.

Figure 17 shows a typical observation of 10,000 data points and was made on a single particle. As explained in previous sections, this intensity distribution is converted

into a height distribution using equation 4. Then, the particle's height histogram was determined and was used in equation 6 to calculate the potential energy of the interactions.

CONSTRUCTION OF POTENTIAL ENERGY PROFILE

The PE profile constructed from the instantaneous distance of separations between the particles and the surface is shown in Figure 18. These profiles were constructed for a single QD-embedded microsphere. During the scattering measurement, we used a band pass filter allowing only the 488 nm excitation light to be captured by the CCD camera. The same protocol explained in Figures 15 and 16 was followed for luminescence measurements.

From the figure, luminescence seems to produce an accurate PE profile of the particle-surface interactions. The potential energy profile matches that of the theoretical PE profile of a single particle. The scattering profile seems to suffer from an anomaly when the particle is near its most probable height. We are exploring the anomaly and its causes. One possible cause for this problem is particle polydispersity as previously discussed.[3]

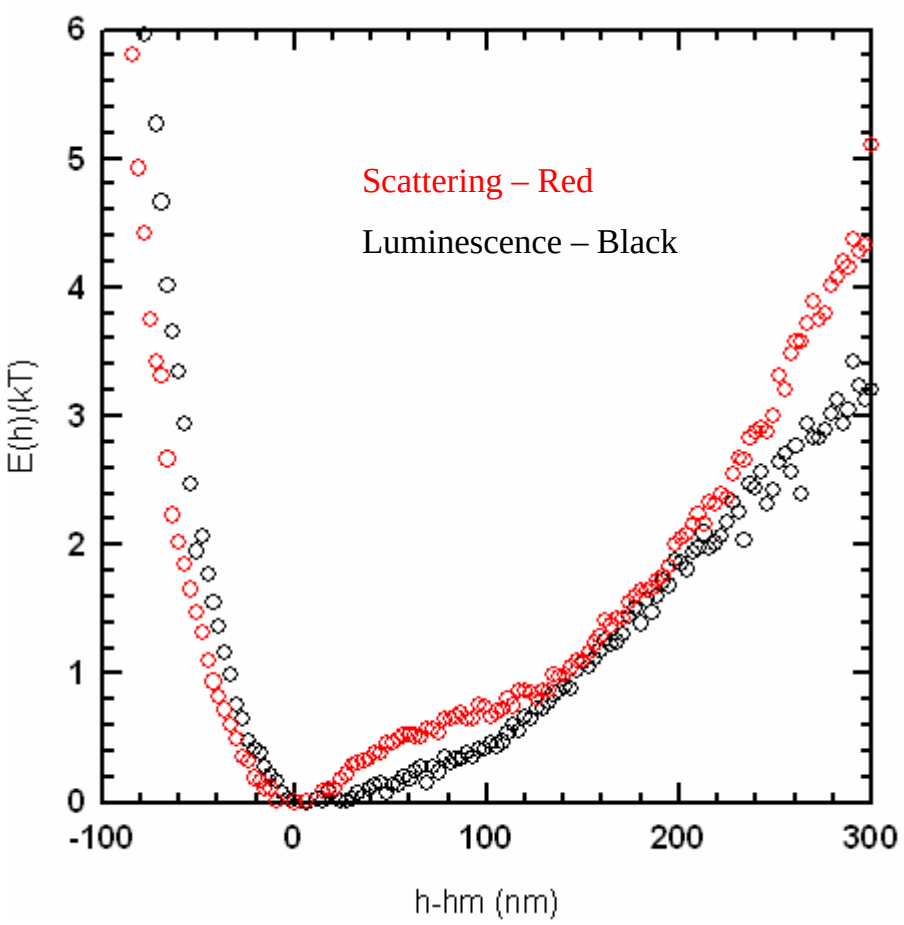

Figure 18. PE Profiles of 4 μm Polystyrene Microspheres Embedded with 590 nm QD's.

SPECTRAL MULTIPLEXING

We have successfully embedded the three different sized quantum dots with emission peaks at 541 nm, 590 nm and 634 nm in 4 μm polystyrene microspheres. A confocal image of microspheres embedded with three different-sized QD's is shown in Figure 19. A single line Ar-ion laser emitting at 488 nm was used to excite the quantum dots of different size.

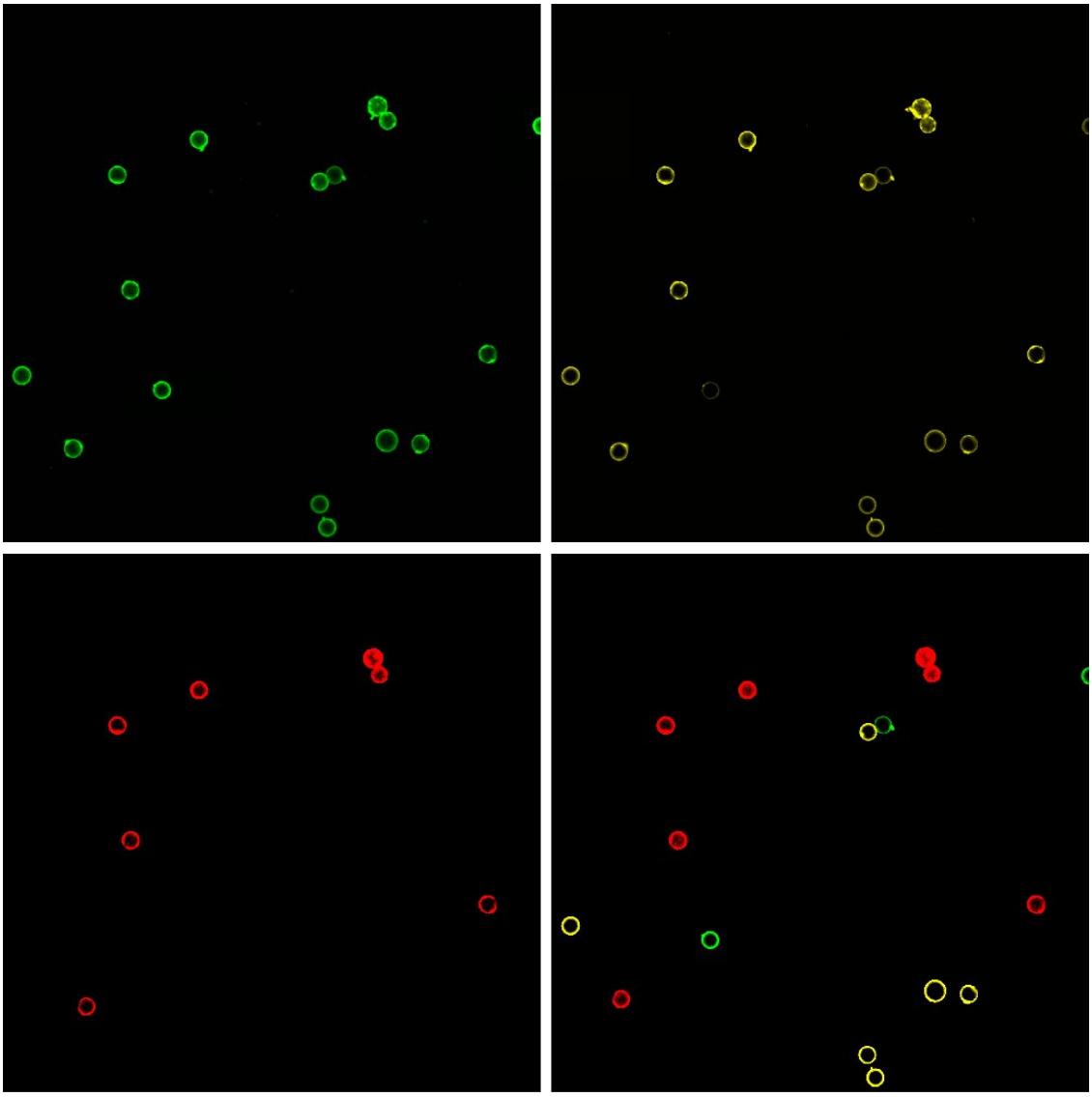

Figure 19. A Three-channel Confocal Microscope Image Showing 4 μm Polystyrene Microspheres Embedded with Different-sized QD's.

The top two images and the bottom-left image in Figure 19 were captured from three-channels with appropriate optical filters to allow only a specific spectral band. The first channel (top-left) has a long pass filter with 505 nm cut off with the second (top-right) and third channels (bottom-left) possessing long pass filters with 560 and 650 nm

as cutoff wavelengths. The bottom-right part of the image shows all the particles that are present in the sample.

As seen in the image, the 505 nm channel allows emission from QD-incorporated microspheres of all emission peaks since we used 541 (green), 590 (yellow) and 634 nm (red) peak emission QD's. The second channel with a 560 nm filter blocks the signal from 541 nm QD-tagged microspheres and allows the signal due to the emission of 590 and 634 nm QD-tagged microspheres. The third channel allows only the luminescence due to the emission of 634 nm QD-embedded microspheres.

For easy viewing, the spherical particles are colored according to their emission wavelength, without changing their position, which is shown in the bottom-right part of Figure 19.

It should be noted that there is some cross-talk in the spectra of the QD-tagged microspheres. All three 541 nm dots-embedded microspheres seem to luminesce at a low intensity in the second channel despite the channel having a 560 nm long pass filter. If we look at Figure 13 showing the emission spectra of the three QD's used in this experiment, the green dots seem to have a normalized intensity of ~0.4 at 560 nm which explains their luminescence in the second channel. The yellow QD's do not suffer a similar spectral overlap with the 650 nm filter as their intensity is significantly low at that point in the emission spectrum. Using QD's with no or very low spectral overlap and the usage of optimized filters should result in higher-quality spectral multiplexing.

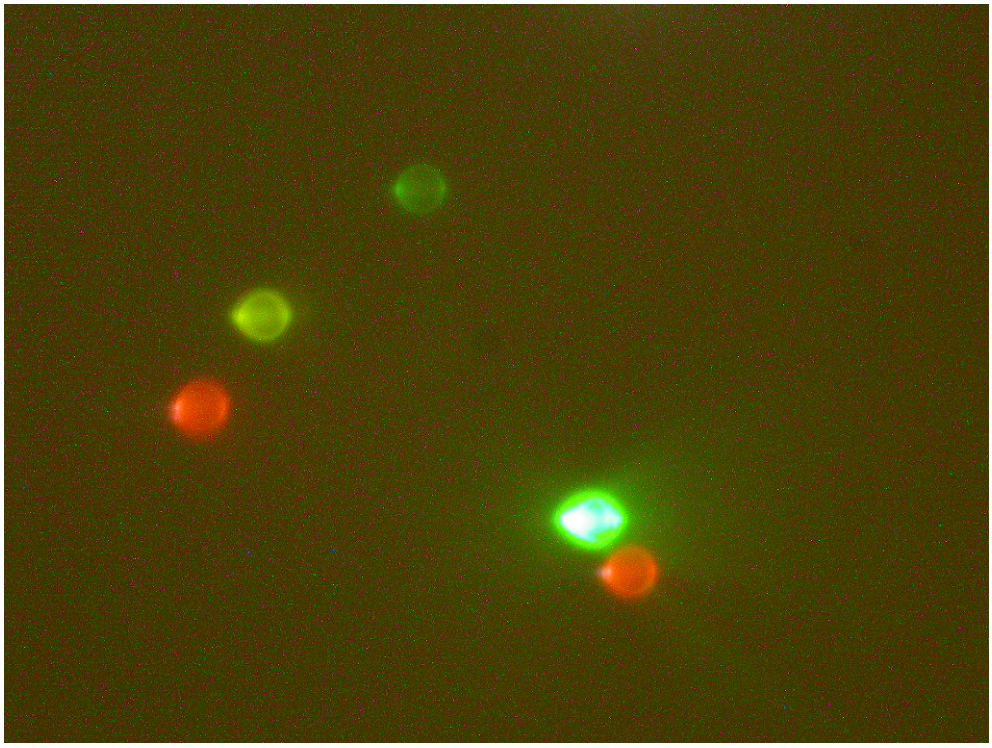

Figure 20. DCPM Image of Polystyrene Microspheres Embedded with 541 nm, 590 nm and 634 nm QD's.

Figure 20 shows the simultaneous EW excitation of three different colored QD-tagged microspheres. It has to be noted that this a true color image taken by a digital color camera fitted with a long pass filter to reject the 488 nm excitation light. The direction of the evanescent wave excitation is from left to right. The brightest microsphere seen in the image is very close to the surface where the intensity of excitation is very high. One of the particles tagged by 541 nm QD's (green) looks very dim suggesting that it is far from the surface, because of the exponential decay of the EW from the surface.

As seen above, incorporating these QD-embedded microspheres into the DCPM system resulted in multiplexed optical coding due to the optical properties of quantum dots. The three different emission wavelengths can be clearly distinguished by the naked eye suggesting that the spectral overlap between the QD's has been minimal. Further refinement of the QD synthesis process can lead to a higher number of spectrally separated QD's resulting in the simultaneous monitoring of a large number of particles. This would enable high resolution force measurements between multiple functionalized particles and a surface and provides a novel tool for the investigation of bio-molecular interactions.

SUMMARY AND CONCLUSION

We have successfully developed a tool to simultaneously monitor multiple particle-surface interactions at a very high force resolution. Imaging measurements show the coded microspheres have a highly uniform QD ring and are bright and can be detected accurately. Also, the potential energy profiles due to luminescent particles demonstrate an alternative to scattering measurements in DCPM.

The narrow and symmetric emission spectra of QD's along with their broad absorption spectra make spectral multiplexing a viable technique. The ability of DCPM to exhibit nanometer spatial resolution with the ability to detect potentials on the order of kT makes it an ideal technique to simultaneously measure force interactions of multiple functionalized microspheres.

The ability of QD's to resist photobleaching is critical to this technique. While organic fluorophores lose their fluorescence merely seconds after excited by high intensity light, quantum dots are resistant to photobleaching and their luminescence remains unaffected even after 30 minutes. This is especially important in studying the interactions of particles and surface using DCPM where a large number of samples are required to construct the potential energy profile of interactions.

Functionalizing the quantum dot labeled microspheres with bio-molecules will lead to simultaneous monitoring of interactions between bio-molecules and the surface with a force sensitivity of 10^{-14} N. We feel this technique will provide a novel tool in understanding the different forces and their effects in human physiology.

FUTURE WORK

INCORPORATION OF QUANTUM DOTS INTO CORE-SHELL SILICA MICROSPHERES

Introduction

This section shows an alternative procedure to perform spectral multiplexing with QD's. Here, the CdSe quantum dots were incorporated into silica microspheres as opposed to the polystyrene microspheres discussed previously in this work.

Motivation

Quantum dots used to tag polystyrene microspheres are not chemically bound to the internal surface of the microsphere. So, when submerged in non-polar solvents, the quantum dots can leak out.[45] Here, QD's have been attached to the surface of silica microspheres and then incorporated into a silica shell as described by Chan et al.[46] It is a robust procedure and most importantly, the tagged microspheres are stable in a variety of polar and non-polar solvents.

Methods

The CdSe/TOPO quantum dots suspended in toluene were washed several times with butanol and hexane to get rid of the TOPO layer. The quantum dots were then dried in vacuum. 135 mg of CdSe quantum dots was mixed with 1000 mg anhydrous ethanol and 150 mg 3-aminopropyltrimethoxysilane (APS) to form a suspension of quantum dots. 60 mg of 5-amino-1-pentanol (AP) was added to this solution which was subsequently heated at 40^0 C for 30 minutes. This step resulted in the capping of the

quantum dot surface with APS and AP on the surface of the quantum dots. The capping with APS and AP was done under nitrogen blanket.

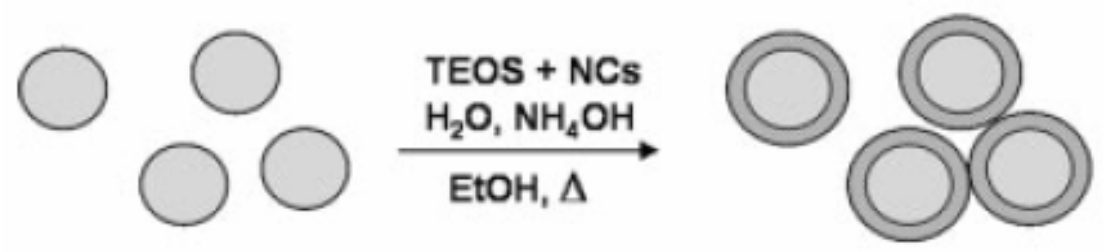

Figure 21. Reaction Scheme of QD Incorporation into Core-Shell Silica Microspheres.[46]

Addition of 10 μL of this quantum dot solution to 30 mg silica microspheres 2.4 μm in diameter (10%, purchased from Bangs Labs, Fishers, IN) resulted in quantum dots attached to the surface of silica microspheres. To this solution, 16 mg hydroxypropyl cellulose dispersed in 10 mL ethanol was added and this was followed by the addition of 50 μL water, 50 μL NH_4OH and 150 μL tetra-ethoxy silane (TEOS). The mixture was then immersed in an oil bath at 75^0 C for 4 hours while stirring.

This process resulted in the formation of silica shell around the quantum dot-coated microspheres. The silica/silica-quantum dot solution was cleaned 4 times with ethanol and was finally re-dispersed in ethanol. Figure 21 illustrates the reaction scheme where NCs correspond to the CdSe nanocrystals and the other terms assume their usual meaning.[46]

Preliminary Results

Figure 22 shows the QD-tagged core-shell silica microspheres. The QD's used were CdSe quantum dots of 606 nm emission peak. The microspheres used were 2.4 μm in diameter. The excitation source was a 488 nm Ar-ion laser and a long pass filter of 505 nm cutoff wavelength was employed to block the excitation wavelength and allow the QD luminescence.

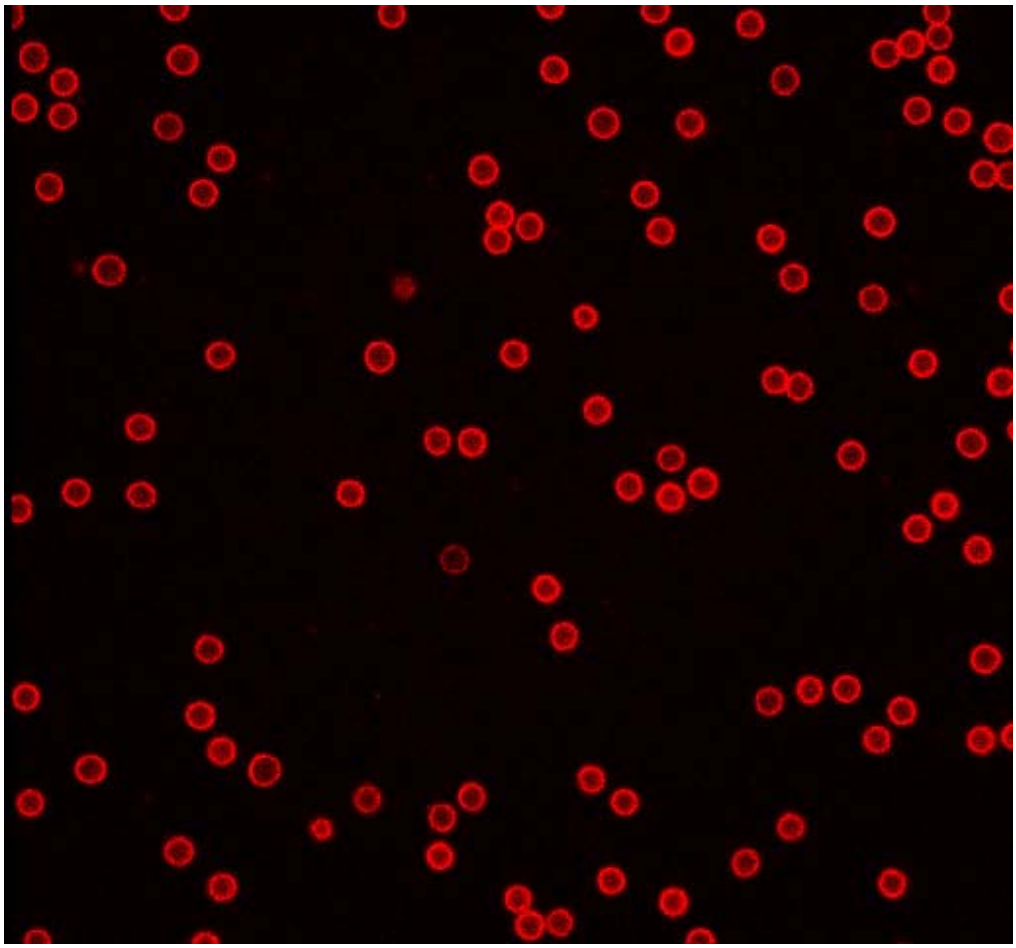

Figure 22. Confocal Image of 2.4 μm Core-Shell Silica Microspheres Tagged by 606 nm QD's.

These microspheric particles look monodisperse under the microscope. Also, the amount of QD's incorporated can be increased by a series of successive silica coatings without a significant loss of monodispersity. Their stability in different kinds of solvents along with their photostability and brightness will further improve the DCPM-QD tagged microsphere system. Further investigations will look at the performance improvement when spectrally multiplexed silica microspheres are used in the DCPM system.

REFERENCES

1 Prieve, D.C. *Adv. Colloid Interface Sci.* **1999**, *82*, 93.

2 Bevan, M.A.; Prieve, D.C. *Langmuir* **1999**, *15*, 7925.

3 Allen, A.L. *Modeling Scattered Intensities for Multiple Particle TIRM Using Mie Theory*; Master's thesis, Texas A&M University, College Station, TX, 2006.

4 Kittel, C. *Introduction to Solid State Physics*, 5th ed.; John Wiley and Sons: New York, 1976.

5 Nave, C.R., "Energy Bands for Solids"; Retrieved on October, 2006 from http://hyperphysics.phy-astr.gsu.edu/hbase/solids/band.html

6 Klimov, V.I. *Los Alamos Science* **2003,** *28*, 214.

7 Haug, H.; Koch, S.W. *Quantum Theory of the Optical and Electronic Properties of Semiconductors*, 3rd ed.; World Scientific Publishing Co.: Hackensack, NJ, 1990: p 386.

8 Murray,R., "Quantum Dot Research – Introduction to Quantum Dots"; Retrieved on October, 2006 from http://www.imperial.ac.uk/research/exss/research/semiconductor/qd/intro.htm

9 Peyghambarian, N.; Koch, S.W.; Mysrowicz, A. *Introduction to Semiconductor Optics*, Prentice Hall: Upper Saddle River, NJ, 1993.

10 Herz, E. *Colloidal Semiconductor Nanocrystals: A Study of the Syntheses of and Capping Structures for CdSe*; Master's thesis, Virginia Polytechnic Institute and State University, Blacksburg, VA, 2003.

11 Alivisatos, A.P. *Science* **1996**, *271*, 933.

12 Goldstein, L.; Glas, F.; Marzin, J.Y.; Charasse, M.N.; Le Roux, G. *Appl. Phys. Lett.* **1985**, *47*, 1099.

13 Snyder, C.W.; Orr, B.G.; Kessler, D.; Sander, L.M. *Phys. Rev. Lett.* **1991**, *66*, 3032.

14 Zhu, J.; Liao, X.; Zhao, X.; Wang, J. *Materials Letters* **2001,** *47*, 339.

15 Peng, Z.A.; Peng, X. *J. Am. Chem. Soc*. **2001**, *123*, 1389.

16 Murray, C.B.; Norris, D.J.; Bawendi, M.G. *J. Am. Chem. Soc*. **1993**, *115*, 8706.

17 Murray, C.B.; Kagan, C.R.; Bawendi, M.G. *Annu. Rev. Mater. Sci.* **2000**, *30*, 545.

18 Hines, M.A.; Guyot-Sionnest, P. *J. Phys. Chem.* **1996**, *100*, 468-471.

19 Efros, AI.L.; Rohen, M. *Annu. Rev. Mater. Sci.* **2000**, *30*, 475.

20 Nirmal, M.; Dabbousi, B.O.; Bawendi, M.G.; Macklin, J.J.; Trautman, J.K.; Harris, T.D.; Brus, L.E. *Nature* **1996**, *383*, 802.

21 Smith, A.M.; Nie, S. *Analyst* **2004**, *129*, 672.

22 Nirmal, M.; Brus, L.E. *Acc. Chem. Res.* **1999**, *32*, 407.

23 Han, M.; Gao, X.; Su, J.Z.; Nie, S. *Nat. Biotech.* **2001**, *19*, 631.

24 Spiro, A.; Lowe, M.; Brown, D. *Appl. Env. Microbio.* **2000**, *66*, 4258.

25 Wang, L.; Yang, C.; Tan, W. *Nano Letters* **2005**, *1*, 37.

26 Xu, H.; Sha, M.Y.; Wong, E.Y.; Uphoff, J.; Xu, Y.; Treadway, J.A.; Truong, A.; O'Brien, E.; Asquith, S.; Stubbins, M.; Spurr, N.K.; Lai, E.H.; Mahoney, W. *Nucleic Acids Res.* **2003**, *31*, e43.

27 Meissner, K.E.; Herz, E.; Kruzelock, R.P.; Spillman, W.B. Jr. *Phys. Stat. Sol. (c)* **2003**, *0*, 1355.

28 Wu, X.; Liu, H.; Liu, J.; Haley, K.N.; Treadway, J.A.; Larson, J.P.; Ge, N.; Peale, F.; Bruchez, M.P. *Nat. Biotech.* **2003**, *21*, 41.

29 Dahan, M.; Laurence, T.; Pinaud, F.; Chemla, D.S.; Alivisatos, A.P.; Sauer, M.; Weiss, S. *Optics Letters* **2001**, *26*, 825.

30 Derfus, A.M.; Chan, W.C.W.; Bhatia, S.N. *Nano Letters* **2004**, *4*, 11.

31 Kirchner, C.; Liedl, T.; Kudera, S.; Pellegrino, T.; Javier, A.M.; Gaub, H.E.; Stolzle, S.; Fertig, N.; Parak, W.J. *Nano Letters* **2005,** *5*, 331.

32 International School of Photonics, “Fiber Optic Sensors”; Retrieved on October, 2006 from http://www.photonics.cusat.edu/Research_Fiber%20Sensors_EW.html

33 Chew, H.; Wang, D.S.; Kerker, M. *Applied Optics* **1979**, *18*, 2679.

34 Steiner, G. *Anal. Bioanal. Chem.* **2004**, *379*, 328.

35 Fulton, R.J.; McDade, R.L.; Smith, P.L.; Kienker, L.J.; Kettman, J.R. Jr. *Clin. Chem*. **1997**, *43*, 1749.

36 Diaz, M.R.; Boekhout, T.; Theelen, B.; Bovers, M.; Cabanes, F.J.; Fell, J.W. *Journal of Medical Microbiology* **2006**, *55*, 1197.

37 Bruchez, M. Jr.; Moronne, M.; Gin, P.; Weiss, S.; Alivisatos, A.P. *Science* **1998**, *281*, 2013.

38 Chan, W.C.W.; Nie, S.M. *Science* **1998**, *281*, 2016.

39 Mitchell, G.P.; Mirkin, C.A.; Letsinger R.L. *J. Am. Chem. Soc.* **1999**, *121*, 8122.

40 Mattoussi, H.; Mauro, J.M.; Goldman, E.R.; Anderson, G.P; Sundar, V.C.; Mikulec, F.V.; Bawendi, M.G. *J. Am. Chem. Soc*. **2000**, *122*, 12142.

41 Pathak, S.; Choi, S.-K.; Arnheim, N.; Thompson, M.E. *J. Am. Chem. Soc.* **2001**, *123*, 4103.

42 Dickerson, B.D. *Organometallic Synthesis Kinetics of CdSe Quantum Dots;* Ph.D. dissertation, Virginia Polytechnic Institute and State University, Blacksburg, VA, 2005.

43 Wu, H-J.; Pangburn, T.O.; Beckham, R.E.; Bevan, M.A. *Langmuir* **2005**, *21*, 9879.

44 Crocker, J. C.; Grier, D. G. *J. Colloid Interface Sci.* **1996**, *179*, 298.

45 Gao, X.; Nie, S. *J. Phys. Chem. B* **2003**, *107*, 11575.

46 Chan, Y.; Zimmer, J.P.; Stroh, M.; Steckel, J.S.; Jain, R.K.; Bawendi, M.G. *Advanced Materials* **2004**, *16*, 2092.

VITA

Shankarapandian Muthukumar was born in Tuticorin, India. He attended school and college in Chennai, India and received his Bachelor of Engineering degree in electronics & communication engineering from University of Madras in 2004. He joined Texas A&M University in August 2004 and received his Master of Science degree in biomedical engineering in May 2007.

He can be contacted at Shankarapandian Muthukumar, c/o Dr.Kenith Meissner, Department of Biomedical Engineering, 335 F Zachry Engineering Center, 3120 TAMU, College Station, TX-77843.